Developmental Cognitive Neuroscience 64 (2023) 101326

Contents lists available at ScienceDirect

Developmental Cognitive Neuroscience

journal homepage: www.elsevier.com/locate/dcn

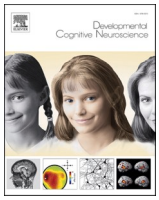

Developmental coupling of brain iron and intrinsic activity in infants during the first 150 days

Lanxin Ji [a,*], Youngwoo Bryan Yoon [a], Cassandra L. Hendrix [a], Ellyn C. Kennelly [b], Amyn Majbri [a], Tanya Bhatia [a], Alexis Taylor [b], Moriah E. Thomason [a,c,d]

[a] Department of Child and Adolescent Psychiatry, New York University School of Medicine, New York, NY, USA
[b] Department of Psychology, Wayne State University, USA
[c] Department of Population Health, New York University School of Medicine, New York, NY, USA
[d] Neuroscience Institute, New York University School of Medicine, New York, NY, USA

ARTICLE INFO

Keywords:
Infant
Brain development
Brain iron
R2*
ALFF
Linked ICA

ABSTRACT

Brain iron is vital for core neurodevelopmental processes including myelination and neurotransmitter synthesis and, accordingly, iron accumulates in the brain with age. However, little is known about the association between brain iron and neural functioning and how they evolve with age in early infancy. This study investigated brain iron in 48 healthy infants (22 females) aged 64.00 ± 33.28 days by estimating R2 * relaxometry from multi-echo functional MRI (fMRI). Linked independent component analysis was performed to examine the association between iron deposition and spontaneous neural activity, as measured by the amplitude of low frequency fluctuations (ALFF) by interrogating shared component loadings across modalities. Further, findings were validated in an independent dataset (n = 45, 24 females, 77.93 ± 26.18 days). The analysis revealed developmental coupling between the global R2 * and ALFF within the default mode network (DMN). Furthermore, we observed that this coupling effect significantly increased with age ($r = 0.78$, $p = 9.2e\text{-}11$). Our results highlight the importance of iron-neural coupling during early development and suggest that the neural maturation of the DMN may correspond to growth in distributed brain iron.

1. Introduction

Iron is an essential metabolic cofactor that plays a crucial role in regulating neural activity. It is involved in many neural processes, including myelination, the synthesis and metabolism of neurotransmitters such as dopamine and serotonin, also the electron transport chain, which provides energy to neurons to maintain their activity (Rouault, 2013; Ward et al., 2014b). In neuroimaging studies of adults and aging populations, disruptions in neural circuits have been observed when excessive brain iron accumulation and poorer cognitive performance are present, suggesting a close relationship between iron and neural function. For example, striatal iron concentration is negatively associated with neural activity both in resting-state (Salami et al., 2018) and during cognitive tasks (Kalpouzos et al., 2017; Zachariou et al., 2020). In the context of human development, iron and functional networks change throughout childhood to support neurocognitive maturation (Larsen and Luna, 2015; Ning et al., 2014). Studies of typically developing children have shown that both brain iron and neural activity are linked to various domains of cognitive performance (Larsen et al., 2020a), including working memory (Darki et al., 2016; Sala-Llonch et al., 2012), processing speed (Hect et al., 2018; Wang et al., 2022), and IQ (Carpenter et al., 2016; Hect et al., 2018). Deficient brain iron concentration and altered neural activity have also reliably been reported in populations with neurodevelopmental disorders, including attention deficit hyperactivity disorder (ADHD) (Adisetiyo et al., 2014a; Cortese et al., 2012b; Yu-Feng et al., 2007) and autism (Karavallil Achuthan et al., 2023; Tang et al., 2021). While these observations suggest a relationship between iron and neural function, it remains unclear what role iron may be playing in the initial early development of neural functioning, as well as how this role evolves with age.

Early infancy is a critical developmental phase characterized by heightened plasticity, as the brain undergoes rapid growth and expansion (Knickmeyer et al., 2008). During this phase, there is a surge of axonal myelination and dendritic arborization, and rapid accruement of functional synaptic contacts (Brody et al., 1987; Petanjek et al., 2011), all of which heavily rely on brain iron (Connor and Menzies, 1996). MRI

* Correspondence to: One Park Avenue, 8th Floor, New York, NY 10016, USA.
E-mail address: lanxin.ji@nyulangone.org (L. Ji).

https://doi.org/10.1016/j.dcn.2023.101326
Received 25 July 2023; Received in revised form 30 October 2023; Accepted 15 November 2023

studies in infants show that iron continually accumulates in deep gray matter from the perinatal period through to adulthood (Cabral et al., 2023a; Cabral et al., 2023b; Ning et al., 2019; Raab et al., 2022; Zhang et al., 2019). In infancy, cord ferratin levels are found to be related to motor and cognitive behavior at 5 years of age (Tamura et al., 2002), and lower cognitive function caused by iron deficiency during infancy persist even after iron therapy (Georgieff, 2011; Lozoff et al., 2006). These findings suggest the pivotal role of iron during infancy in setting long-term developmental trajectories in cognitive function. As iron is a critical metabolic cofactor for core cellular processes, the increasing demand of iron aligns with the continuing increase of brain metabolism in development (Kuzawa et al., 2014). At the same time, brain neural activity, is also sensitive to developmental change and closely linked to brain metabolism (Aiello et al., 2015). The neural activity during rest has been shown to increase from 2 to 6 years of age in regions within the Default Mode Network (DMN) and frontoparietal network, and to decrease in the superior parietal lobe and superior temporal gyrus across this age range (Long et al., 2017), though the neural activity changes prior to the age of 2 years remain less characterized. Given the vital metabolic role of iron and the close relationship between neural and metabolic activity, we hypothesize that there is an association between iron and neural activity, partially driven by metabolic function. Investigating the relationship between brain iron and neural activities during early infancy could provide insight into the etiology of functional networks and inform novel insight into the processes that guide brain organization during early developmental stages.

To evaluate the paring between iron and neural activity, proxies for both regional iron concentration and brain activity are needed. Several magnetic resonance imaging (MRI) methods are sensitive to brain iron including the transverse relaxation rate R2* measured from MR images acquired at different echoes, and quantitative susceptibility mapping (QSM) (Haacke et al., 2005; Schenck and Zimmerman, 2004). Both R2* and QSM have shown high reproducibility (Hametner et al., 2018) and strong correlations with postmortem iron measures (Langkammer et al., 2010; Langkammer et al., 2012). These techniques are widely used to study age-related changes of iron and to serve as a marker of individual differences as well as dysfunction (Hect et al., 2018; Larsen et al., 2020a). With regard to measurement of neural activity, the amplitude of low-frequency fluctuations (ALFF) in resting-state functional MRI (fMRI) blood oxygen level dependent (BOLD) signal can be used as a proxy (Biswal et al., 2010; Zang et al., 2007; Zou et al., 2008). ALFF is defined as the power within the low-frequency range (around 0.01–0.1 Hz), for the time course of each voxel (Zang et al., 2007). The rationale for the use of ALFF is based on the assumption that slow fluctuations in neural activity are a fundamental feature of the resting brain, and their presence is essential for determining correlated activity between brain regions (Tomasi and Volkow, 2018; Zuo et al., 2010). ALFF varies across brain regions and between subjects and is highly correlated with simultaneously recorded maps of glucose metabolism, making it a strong proxy for neural activity (Aiello et al., 2015).

In the present study, we employed BOLD ALFF and R2* MRI techniques to provide the first empirical evaluation of intrinsic cortical activity and brain iron coupling across the first 150 days of life. Multi-echo fMRI was used to simultaneously acquire both metrics, as it provides a unique opportunity to examine the two measures concurrently. By exploring the link between brain iron and neural activity during this crucial developmental period, we could gain understanding of the role of iron in driving brain functional organization during the early stages of development. We hypothesized that brain regions with higher metabolism, such as the DMN and the deep gray matter, would exhibit a coupled increase in R2* and ALFF, and that this effect would be strengthened with advancing age.

2. Methods and materials

2.1. Participants

2.1.1. Detroit cohort

Sixty-three MRI scans were collected from 57 healthy infants (28 females, 25–144 days after birth) between 2013 and 2018 as part of the Perinatal Imaging of Neural Connectivity (PINC) project, from the Detroit Medical Center (Detroit data). Eligibility criteria included singleton pregnancy, maternal age 18–40, no suspected central nervous system abnormality as determined by 20-week ultrasound, and no contraindication for MRI. The Wayne State University Institutional Review Board approved all study procedures, and informed written consent was provided by participating pregnant people.

2.1.2. New York cohort

To evaluate the reproducibility of our findings, we employed an independent dataset in this study including 45 infants (24 females, 38–154 days after birth) drawn from the COVID-19 Perinatal Experiences (COPE) cohort, recruited across the New York area during 2021–2023. Eligibility criteria included parent over 18 years old, lack of any contraindications for infant MRI, and infant cardiac abnormalities. The New York University Institutional Review Board approved the study procedures and informed consent was provided by participants using REDCap.

2.2. MRI acquisition protocol

2.2.1. Detroit cohort

Participants were scanned on a 3T Siemens Verio scanner, with a 32-channel head coil, using one of three sets of acquisition parameters, as detailed below. (i) 12-min multi-echo (ME) fMRI (360 volumes): TR = 2000 ms; TE = 13, 26.07, 39.14 ms; flip-angle: 83 degrees; slice-gap: none; voxel-size: 3.5 × 3.5 × 3.5 mm^3; matrix-size: 64 × 64 × 39 voxels (N = 11 scans). (ii) 12-min multi-band (MB) ME fMRI scan (480 volumes): TR = 1500 ms; TE = 15, 30.72, 46.44 ms; flip-angle: 83 degrees; slice-gap: none; voxel-size: 2.9 × 2.9 × 2.9 mm^3; matrix-size: 64 × 64 × 48 voxels, multi-band factor = 2 (N = 7 scans). (iii) 7-min MB ME fMRI scan (420 volumes): TR = 1000 ms; TE = 14.6, 36.68, 58.76 ms; flip-angle: 52; slice-gap: none; voxel-size: 2.5 × 2.5 × 2.5 mm^3; matrix-size: 80 × 80 × 44 voxels, multi-band factor = 4 (N = 45 scans).

2.2.2. New York cohort

Participants were scanned on a 3T Siemens Prisma scanner, with a 32-channel head coil. FMRI data was collected with following acquisition parameters: TR = 2000 ms; TE = 13, 30.88, 48.16, 65.44 ms; flip-angle: 75 degrees; slice-gap: none; voxel-size: 2.8 × 2.8 × 2.8 mm^3; matrix-size: 68 × 68 × 44 voxels.

2.3. FMRI Pre-processing

We employed a combination of functions provided by FSL (Jenkinson et al., 2012, https://fsl.fmrib.ox.ac.uk/fsl/fslwiki/) and SPM (Friston, 2003, https://www.fil.ion.ucl.ac.uk/spm/) software to preprocess the multi-echo fMRI data. The infant brain was extracted using FSL's Brain Extraction Tool (BET, Smith, 2002), and motion correction was estimated based on the first echo via "FSL mcflirt" (Jenkinson et al., 2002). The resulting alignment parameters were applied to the remaining echoes. The root-mean-square of voxel-wise differentiated signal (DVARS) (Power et al., 2012) were estimated based on alignment parameters using fsl_motion_outliers (Jenkinson et al., 2002). Volumes with DVARS greater than 50 were marked as outliers (censored frames). One frame before and two frames after these volumes were flagged as censored frames as recommended in prior literature (Li et al., 2019). FMRI runs with more than half of the volumes labeled as censored frames were excluded.

The motion-corrected data were then denoised using TE-Dependent Analysis (Tedana, (DuPre et al., 2021; Kundu et al., 2012)). In brief, the optimal combination of the three echoes was calculated, and the echoes were merged to produce a single, optimally weighted time series (included in the Tedana package). Principle component analysis was applied to remove thermal noise and a subject-level independent component analysis was then performed to differentiate BOLD signal and noise. This was achieved by well-established characteristics of the T2* signal decay of the BOLD signal and noise. Components classified as noise were discarded, and the remaining components were recombined to construct the optimally combined, denoised timeseries.

Following the Tedana denoising, fMRI images were normalized to the UNC neonatal template (Shi et al., 2017) and smoothed with a 4 mm gaussian kernel using SPM. Additional CompCor denoising of the BOLD timeseries (Behzadi et al., 2007) was performed using CONN toolbox (Whitfield-Gabrieli and Nieto-Castanon, 2012). This process regresses out signals from noise regions in white matter and cerebrospinal fluid (CSF). Within CONN, we computed the amplitude of low-frequency fluctuations (ALFF), which is the average power of low-frequency (0.008–0.09 Hz) fMRI signal, to index the overall level and coherence of intrinsic cortical activity.

T2* maps were automatically generated by Tedana toolbox. In brief, the estimation of T2* involves fitting a monoexponential decay model to the data collected across echoes. T2* corresponds to the rate at which a voxel decays over time, and this rate is related to signal dropout and BOLD sensitivity (Kundu et al., 2012). The warping matrices obtained from the fMRI normalization were then used to convert corresponding T2* maps from individual space to template space.

2.4. R2* quality control

According to existing literature, T2* estimation can be influenced by the presence of macroscopic field gradients (for example, air/tissue interface) (Hernando et al., 2012). In our dataset, we also observed voxels showing T2* values out of the normal range. Thus, a mask excluding unreliable voxels was needed for voxel-level analysis. We first generated a 'T2* reliability' map defined based on classifying each voxel as having a T2* value between 50 and 150 ms in at least 80 % of the total scans (Fig. 1, mask 1). Fifteen subjects were subsequently excluded from further analysis, because their T2* maps had a noise-related spatial

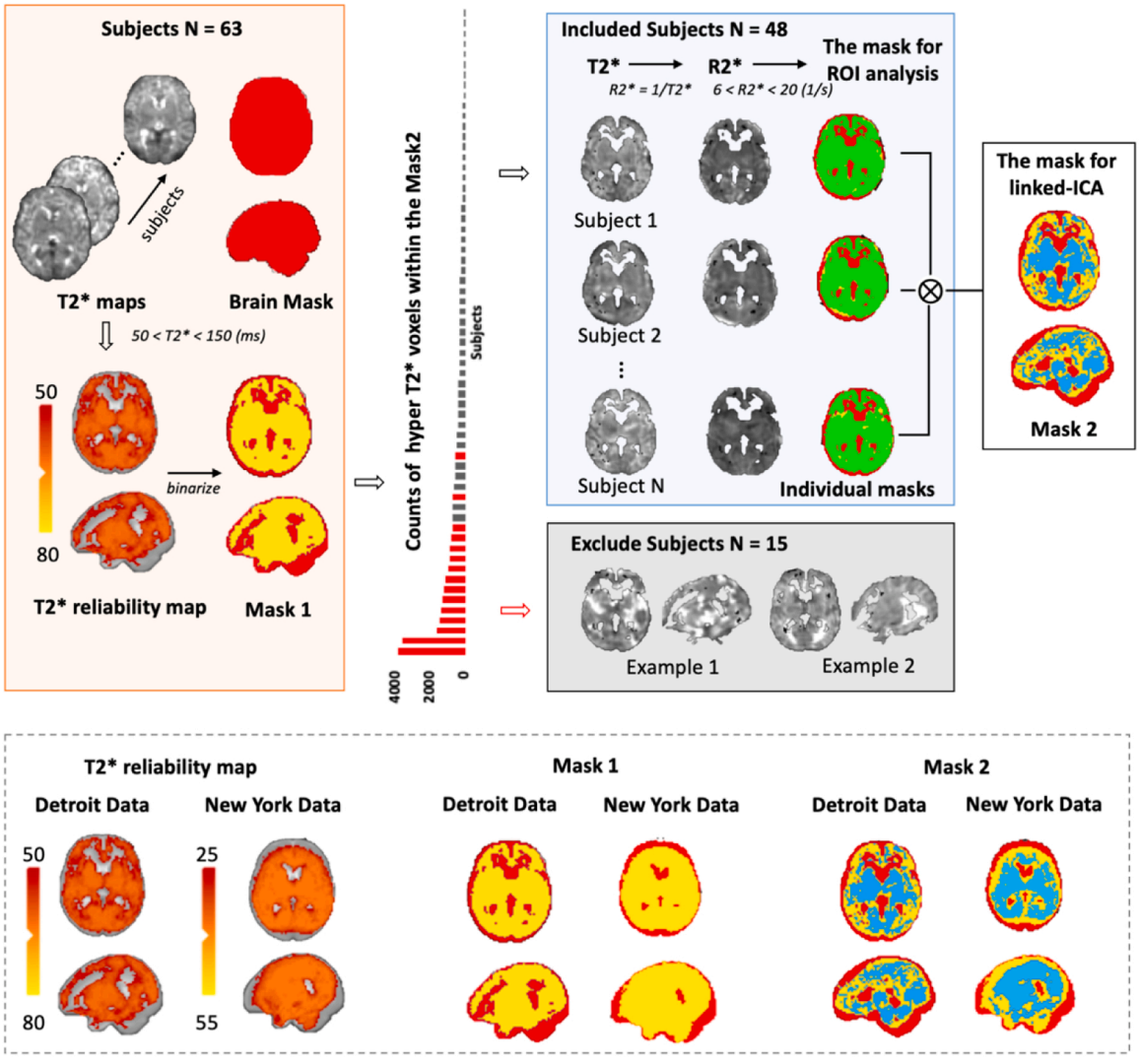

Fig. 1. Pipeline to generate R2* mask. Step1, Mask1(shown in yellow) was defined based on classifying each voxel as having a T2* value between 50 and 150 ms in at least 80 % of the total scans. Step 2, 15 subjects were excluded from further analysis, because their T2* maps had a noise-related spatial distribution and/or because they a high ratio of unreliable voxels overall. Step 3, Mask2 (shown in blue) was generated that contained only the voxels that fell within the reliable range for all 48 subjects retained from Step 2. The Mask 2 is used to refine voxels as input of FLICA analysis. The masks used for the R2* maps in the Detroit and New York Dataset are presented side by side in this figure at the bottom; the blue mask shows the voxels of R2* included in the FLICA.

distribution and/or because of a high ratio of unreliable voxels overall (see excluded cases in the Supplementary Materials Fig. S1). Across the 48 subjects retained after exclusion of n = 15 referenced above, a second mask was generated that contained only the voxels that fell within the reliable range for all subjects, constituting an even more conservative reliability mask. R2* maps were estimated as the reciprocal of T2* (1/T2*). The above pipeline is presented in Fig. 1.

To confirm that our R2* estimates demonstrate anticipated trends with increasing age as reported (Ning et al., 2014), we conducted a Pearson correlation analysis between age and the mean R2* values in several deep gray matter regions. Specifically, we utilized the neonatal Automated Anatomical Labeling (AAL) template (Shi et al., 2017) to define the regions of interest, including the caudate, putamen, pallidum, and thalamus. No significant difference in signal-to-noise ratio (SNR) was found between the preprocessed data with different acquisition parameters.

2.5. Unimodal analysis

Serving as a comparison relative to the cross-modal analysis, two unimodal analyses were conducted to examine the correlation of the R2* and ALFF with age separately. We constructed general linear models (GLMs) in SPM to examine age-dependent changes in brain measure, regressing out the effect of sex and the length of fMRI data. The statistical maps were False Discovery Rate (FDR)-corrected for multiple comparisons.

2.6. Linked Independent Component Analysis (ICA) of ALFF and R2* as they relate to age

Linked Independent Component Analysis (FLICA) was performed to investigate the associations between iron and intrinsic activity in terms of shared component loadings. We submitted masked (mask 2) R2* maps and grey-matter-masked ALFF maps as inputs for FLICA analysis. FLICA is a data-driven approach that automatically decomposes multimodal data into a set of statistically independent components (ICs) and a loading matrix shared across modalities, each column of which indicates the degree of contribution of the corresponding components for each participant (Groves et al., 2011). Thus, each IC has one shared subject loading across modality and each modality has its own spatial map. It is noteworthy that a subject loading may be dominated by a single modality rather than an equal contribution from all modalities of interest. The number of maximum components was set to 20. Statistical analysis for the developmental effect was performed using Pearson correlation analysis between the subject loadings for each component and age. The results were Bonferroni corrected to account for multiple comparisons.

2.7. Reproducibility analysis

We used the same preprocessing strategies to the New York dataset as described above for the Detroit dataset. Demographic characteristics of 45 included subjects are provided in Table 1 and the R2* quality control masks used for the New York dataset are also provided in Fig. 1.

3. Results

3.1. Participants

After fMRI R2* quality control, 48 scans from the Detroit dataset (64.00 ± 33.28 days) were included in the main cross-modality FLICA analysis and 45 scans from the New York Dataset (77.93 ± 26.18 days) were included in the reproducibility analysis. Detailed demographic characteristics of the sample are provided in Table 1. The 48 scans from the Detroit dataset comprises 4 scans using sequence i, 3 scans using sequence ii, and 41 scans using sequence iii. As TR is different across sequences, we provide the distribution of data length after preprocessing in minutes in Supplemental Materials Fig. S2. A sensitivity analysis based on a subset of subjects using sequence iii AND with data length greater than 3 min was performed and replicated results obtained with the entire dataset as described in later sections (see Supplemental Materials Fig. S2).

Table 1
Demographic descriptions of the study population.

	Detroit Dataset (n = 48)		New York Dataset (n = 45)	
	Mean	SD	Mean	SD
Age, days	64.00	33.28	77.93	26.18
Gestational age at birth, weeks	38.78	2.03	38.71	1.58
Birth weight, grams	2685.79	892.51	3179.68	504.06
Number of fMRI volumes	376.85	59.46	400	74.09
Mean DVARS*	32.93	8.64	27.61	16.63
	N	%	N	%
Sex				
Female	22	46	24	53
Male	26	54	21	47
Race				
African American	39	81.25	2	4.44
Asian American	0	0	1	2.22
Bi-racial	8	16.67	5	1.11
Caucasian	0	0	16	35.56
Latina	0	0	2	4.44
Not disclosed	1	2.08	19	42.22

* DVARS, the root mean square of the temporal change of the fMRI voxel-wise signal at each time point.

3.2. Iron accumulates rapidly across the whole brain in early infancy

R2 * of all deep gray matter ROIs significantly increases with age (as shown Fig. 2), replicating previous findings in infants (Cabral et al., 2023a; Ning et al., 2014). Average R2 * value across the whole brain showed an even stronger correlation with age ($r = 0.75$, $p = 1.1e\text{-}09$) compared to the deep gray matter regions, suggesting that iron is accumulated consistently throughout the brain during early development. No sex differences were observed for age-related change in brain iron.

The results of conventional voxel-level unimodal analyses are also shown in Fig. 2. R2* concentrations demonstrated widespread age-related changes in white matter regions and deep gray matter. In contrast, age-related increases in ALFF were only observed in the medial prefrontal cortex, posterior cingulate cortex, and cuneus – gray matter regions that comprise the DMN. In addition, the group average of ALFF and R2* is also provided in the Supplementary Materials Fig. S3.

3.3. ALFF and R2* are closely coupled and change with age

Nine ICs were generated by FLICA analysis and 5 of them shared subject loadings across modalities (Fig. 3). The spatial maps of all 9 components are presented as Fig. S4 in Supplemental Materials. The subject loading of IC1 was significantly associated with increasing age ($r = 0.78$, $p = 9.2e\text{-}11$), indicating that IC1 reflects the age-related changes in iron and intrinsic neural activity. Notably, IC1 highlighted several regions overlapped with the default mode network (DMN), including the posterior cingulate cortex (PCC) and the bilateral medial prefrontal cortex, which are known to be involved in self-referential thought and episodic memory. These findings suggest that the global-wise R2* and ALFF within DMN are increasing with age in a coordinated and synchronized way, suggesting that brain iron may play a pivotal role in forming intrinsic functional networks. In order to confirm that the significant correlation between IC1 and age is not driven by a single modality, we performed separate correlation analyses of age with average R2 * and ALFF within IC1 spatial maps (see Fig. 3 at the box on the right). We confirmed significant correlations with age for both

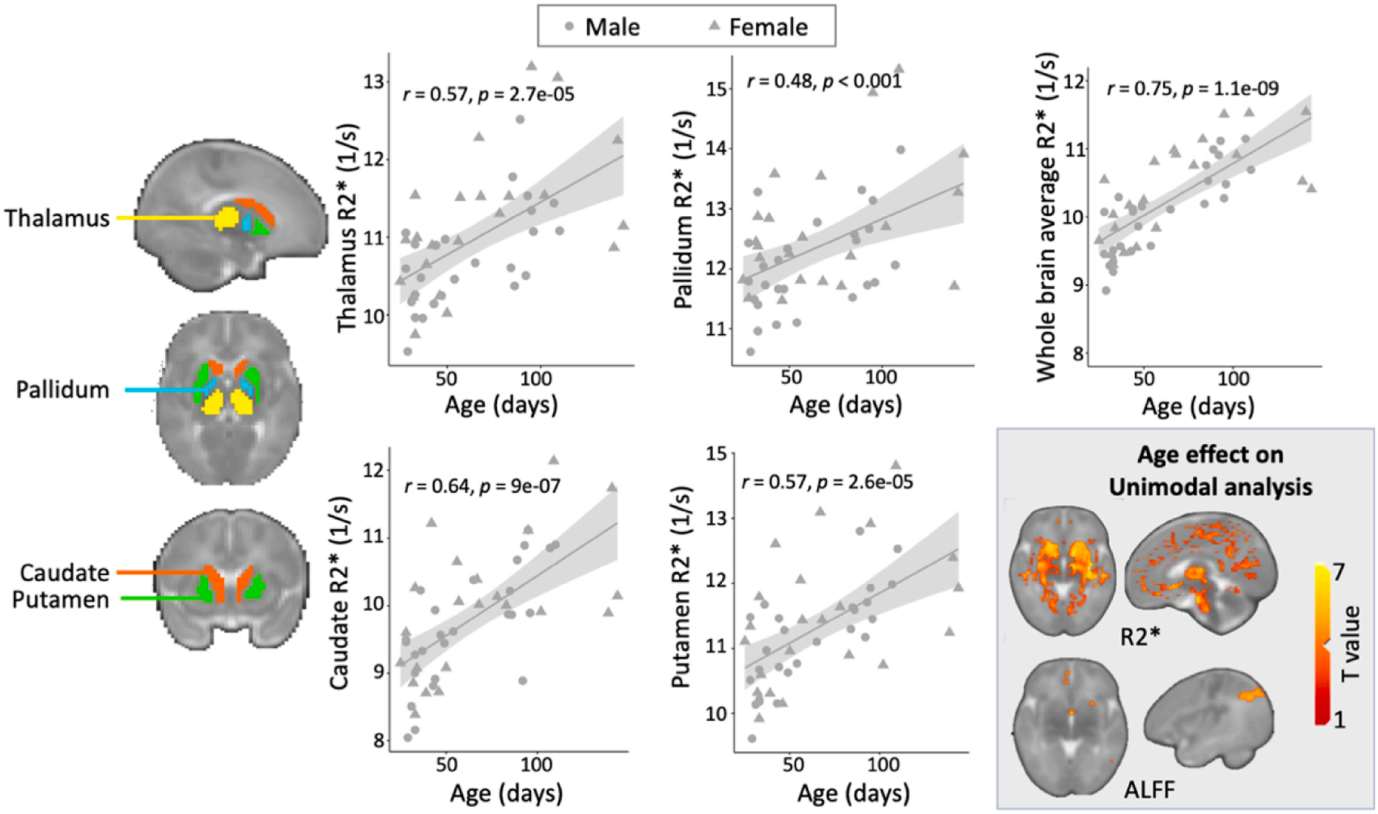

Fig. 2. Age effect on R2* and ALFF with unimodal analysis with increasing age. Pearson correlations between age and the mean R2* values in deep gray matter structures are shown respectively. R2* maps are estimated as the reciprocal of T2* (1/T2*). Regions of interest, including the thalamus, pallidum, caudate, and putamen were defined by the neonatal Automated Anatomical Labeling template. Results of voxel-wise regression analyses are shown in the right bottom box. Voxel-wise regression was performed by constructing general linear models to examine age-dependent changes in each brain measure separately, while regressing out the effect of infant sex and length of fMRI data. The results are false discovery rate (FDR) corrected for multiple comparisons at the significance level of $p < 0.05$.

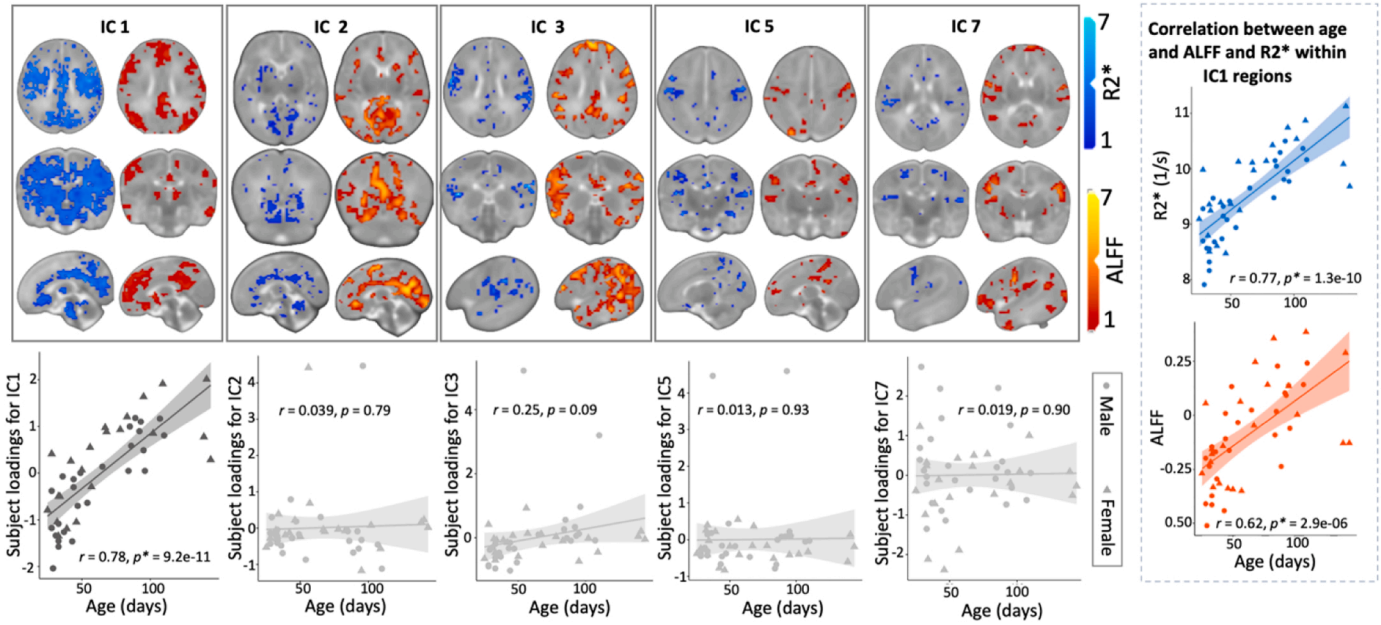

Fig. 3. Coupling between ALFF and R2 * during early brain development. Results of linked independent component analyses (FLICA) and the correlations between the subject loadings of each component (IC) and age are presented. The subject loading of IC1 was significantly associated with increasing age, indicating that the global R2* and ALFF within DMN are increasing with age in a coordinated and synchronized way. In contrast, other components did not show a correlation with age, but did show correspondence R2* and ALFF map overlap in regions of the cingulate (IC2), temporoparietal cortex (IC3, IC7), and motor cortex (IC5), further supporting functional relationships between network connectivity and biological underpinnings of R2 * . In addition, correlation plots between age and R2* and ALFF within IC1 regions are presented in the box on the right.

modalities. Other components did not exhibit a correlation with age, but overlap in R2* and ALFF maps was observed in select areas, including cingulate (IC2), temporoparietal (IC3, IC7), and motor (IC5) regions.

3.4. Replication in an independent dataset

The FLICA analysis on 45 subjects from the independent New York dataset also detected a DMN component and replicated our finding that R2 * and ALFF coupling in this component increase with infant age ($r = 0.67$, $p = 4.5e\text{-}07$, Fig. 4). In addition, we found two ICs (IC4 and IC6) comprised with only a single modality, either R2 * or ALFF, that significantly correlated with age. The spatial maps of these two ICs largely overlapped with IC1, suggesting some collinearity across these ICs ($r = 0.08$ between subject loading of IC1 and IC4; $r = 0.24$ between IC1 and IC6).

We also replicated our previous effect that average R2 * across the whole brain ($r = 0.7$, $p = 1.1e\text{-}07$), and with deep gray matter regions of the thalamus ($r = 0.62$, $p = 4.7e\text{-}06$), caudate ($r = 0.55$, $p = 9.7e\text{-}05$), putamen ($r = 0.54$, $p = 1.1e\text{-}04$), and pallidum ($r = 0.50$, $p = 4.7e\text{-}04$) increased with infant age. The developmental effect was again greatest for the averaged R2 * across the entire brain rather than the deep gray matter regions as was found in analyses of the Detroit sample.

4. Discussion

The current study explored the developmental coupling between brain iron and neural activity in young infants. We found that iron content accumulates rapidly across the whole brain during the first 150 days of postnatal life. Linked independent component analysis revealed a significant interlinked linear increase of the global iron and resting-state neural activity with increasing age, which was not captured using unimodal analyses. Brain regions overlapping with the default mode network (DMN) were highlighted by the cross-modality analysis; specifically, we observed increased low-frequency functional connectivity with age in conjunction with iron accumulation. This study converges on and compliments previous work by providing a more thorough and unbiased exploration of the coupling effects using a the whole-brain, voxel-level approached rather than restricting iron analyses to specific regions.

Adequate iron is essential for contributing to a variety of key neurodevelopmental processes such as myelination, neurotransmitter synthesis, and mitochondrial function (Reinert et al., 2019). Our finding that iron content increases with age in subcortical gray matter regions is consistent with previous studies of neonates focusing on deep gray matter structures (Cabral et al., 2023a; Cabral et al., 2023b; Ning et al., 2014; Raab et al., 2022). Greater iron content supports more advanced cognition in children and adolescents (Daugherty et al., 2015; Larsen et al., 2020a). However, early life iron deficiency can disrupt cognitive development and can induce enduring alterations brain structure and functional networks (Cecilia et al., 2022; Wedderburn et al., 2022). Our data advances understanding by highlighting that significant iron accumulation is observed across the entire brain over infancy and is not

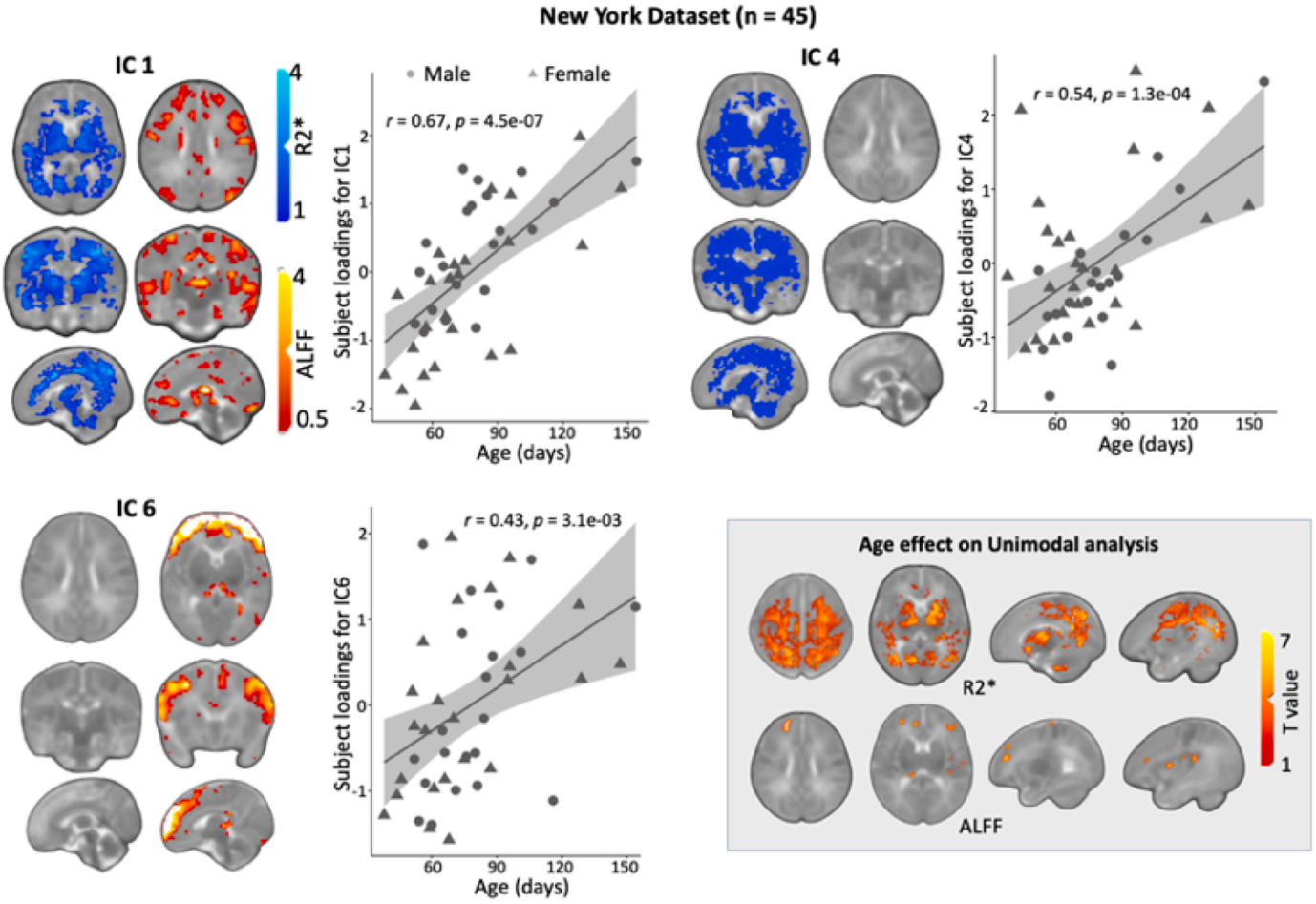

Fig. 4. Testing reproducibility on the independent dataset. Three independent components (IC) showing significant developmental effect are presented. IC1 replicated findings from the Detroit dataset that whole brain R2* coupled with DMN ALFF during early development. Two other ICs (IC4 and IC6) were identified as having increased subject loadings with age. Notably, IC4 R2* shares some regional overlap with IC1. Unimodal results regarding the age effect on the New York dataset are presented with the threshold of $p < 0.05$, FDR corrected.

limited to deep gray matter. Changes in iron included deep gray matter, but also white matter regions including the cingulum bundle and the longitudinal fasciculus, connecting frontal, parietal, and temporal regions. Observed effects in white matter may reflect changes in myelin content occurring across this developmental window.

It is important to examine the underlying role of iron in the context of developmental MRI. While previous MRI studies primarily focus on structural and functional development, little attention has been given to how iron contributes to individual differences in infant brain structure and function. By combining techniques, the current study is able to demonstrate specific associations between neural activity and inferred iron deposition, based on R2*. By showing that these are coupled, we provide support for the mechanistic importance of iron in widespread neurodevelopmental processes, a finding that motivates further opportunities in basic and clinical research in this area. Indeed, this is important in the context of basic science, but also important in promoting the most positive developmental outcomes for infants worldwide. A better understanding of how iron contributes to brain development could inform the development of interventions and treatments that can mitigate the negative effects of iron deficiency or excess, which can have serious consequences on the developing brain.

It is noteworthy that our FLICA analysis isolated iron-ALFF associated regions that overlap with the DMN, a network that is metabolically active during rest and one of the early emerging functional networks (Cao et al., 2017; Gao et al., 2017). High metabolism in these structures is understood to result from elevated neural activity in constituents of this network. Specifically, studies utilizing simultaneous fluorodeoxyglucose positron emission tomography (FDG-PET) and fMRI have shown strong correlations between voxel-wise brain glucose uptake and intrinsic neural activity in DMN regions in healthy subjects (Aiello et al., 2015; Ding et al., 2020; Stiernman et al., 2021). Further, this coupling effect is decreased in patients with cognitive dysfunction, highlighting the importance of the DMN and its associated metabolic and neural activity in supporting healthy brain function. Our findings of strong associations between the whole brain R2* and ALFF in regions that overlap with DMN are consistent with above work describing the high metabolism demand in DMN. Development of DMN in infancy constitutes the most rapid phase of maturation across the life course. Previous studies have shown a primitive and incomplete DMN is present in 2-week-olds, that connectivity of this network shows marked increase over early life, and that the DMN demonstrates spatial extent similar to adults by age of 2 years (Gao et al., 2009). These dramatic developmental changes of DMN likely demand rapidly increasing energy consumption of the brain. Given that R2* has been linked to glucose metabolism and that ALFF and metabolic activity are also linked, we infer that the emergence of DMN is supported by widespread brain iron stores. In fact, adequate brain iron is essential in multiple processes involved in glucose metabolism, including the production of hemoglobin and the delivery of oxygen, which is directly related to the blood oxygen level-dependent (BOLD) signal. Iron is a key component of hemoglobin, and the BOLD signal is dependent on the different magnetic properties of oxygenated and deoxygenated hemoglobin. Our findings provide new insight into understanding of the role of iron in supporting energy-expensive neurological processes, such as the intrinsic neural activity here, which is important for building a comprehensive model of brain functional development.

While the association between brain iron and brain activity in the DMN is expected to relate to metabolic processes, it is also possible that this relationship is uniquely coupled with dopamine function in deep gray matter. Iron co-localizes with dopamine vesicles at the microscopic level and is a necessary co-factor for dopamine synthesis (Ortega et al., 2007; Ward et al., 2014a). In a recent study using *post-mortem* human brain tissue samples, iron distribution in dopaminergic neurons on R2* and susceptibility maps showed a high spatial correspondence to quantitative histological maps (Brammerloh et al., 2021). Additionally, rodent models have demonstrated that brain iron in deep gray matter is linked to dopamine neurobiology and with dopamine-dependent behaviors (Erikson et al., 2000; Lozoff, 2011). In humans, altered iron levels have been widely observed in the dopaminergic-rich structures in children with neurodevelopmental disorders such as ADHD (Adisetiyo et al., 2014b; Cortese et al., 2012a). Combined MRI and PET human studies also support a significant positive association between degree of brain tissue iron, measured using R2*, and quantity of monoamine dopamine transporter VMAT2 (Larsen et al., 2020b). While available data corroborate the colocalization of brain iron and dopamine, inference about the presence of dopamine from MRI should be approached with caution. Here, brain R2* and intrinsic ALFF were used as a means of understanding correspondence of these in early human brain development. An important future direction for the field will be to employ these and other non-invasive imaging techniques (such as QSM and MR Spectroscopy) to better understand interactions across large scale chemical and biological systems, in the context of both typical and atypical early human development.

Utilization of cross-modal techniques is a key component of this study, as it uncovers relationships that might not have been apparent using a single modality. There are several other data-fusion analyses, including joint ICA (jICA (Calhoun et al., 2006)), multi-set canonical correlation analysis (mCCA (Correa et al., 2010)), and approaches combining jICA and mCCA (Sui et al., 2013). We chose linked ICA because it requires fewer assumptions and constraints on the spatial maps. With more rapid acquisition times and expansion of available imaging modalities, we can expect growth in the approaches available for interrogating cross-modal brain features in future years. It is important to note that the outputted components from the data-fusion algorithm indicate the statistical correlation between modalities, but do not necessitate a meaningful biological relationship.

Limitations of this study warrant mention. Infant fMRI data is inherently noisy due to motion effects, small brain size relative to adults, low signal-to-noise ratio, and high maturational variability. As a result, a considerable number of voxels were excluded in our voxel-wise analysis because of low R2* estimate reliability. In our reproducibility analysis, we noticed that the R2* estimates of cortical gray matter regions were even further excluded from the FLCIA analysis, which limited the algorithm's ability to isolate colocalization in R2* and ALFF in cortical gray matter regions. Future studies that include higher-quality estimates of iron in cortical regions may provide more precise spatial linkage between the two measures. Another potential concern relates to potential circularity in our approach; the ALFF estimation from the optimally combined data across echoes could be linked to R2*. This association arises from the slightly higher weighting of the first echo and lower weighting of the last echo when combining data across echoes in older infants. With a roughly estimation of the equivalent TE for the youngest and oldest infants, we anticipate minimal effect of the weight difference on ALFF. Future studies using an independent sequence such as QSM, may further address this concern. The equivalent TEs fall within the range (40–50 ms) typically selected for single-echo sequences in infant studies, suggesting that our ALFF from multi-echo data is comparable to those derived from single-echo data (Fransson et al., 2009; Fransson et al., 2010). To address the potential circularity issue, we conducted an additional analysis by splitting data of 4 subjects to halves. We recalculated ALFF and T2* (reciprocal of R2*) for each half and find high reliability across the two halves within subjects (see supplementary materials Fig. S5). However, it's necessary to acknowledge that due to the nature of optimal combination of multi echoes, variations in R2* across subjects do introduce some degree of variance in multi-echo ALFF, though the impact is minimal as discussed.

CRediT authorship contribution statement

Conceptualization, LJ, YBY, and MET; methodology, LJ, and MET; data collection: CLH, ECK, and AT; investigation, LJ and MET; validation, LJ; data curation, ECK, AM, TB and AT; formal analysis, LJ; writing

– original draft, LJ; writing – review & editing, MT, YBY, and CLH; funding acquisition, MET; resources, MET; visualization, LJ; supervision, MET.

Declaration of Competing Interest

The authors have no competing interests.

Data Availability

This paper analyzes existing available data from the Perinatal Imaging of Neural Connectivity (PINC) project and the COVID-19 Perinatal Experiences (COPE) cohort. The data and code used in this study will be made available via https://ndar.nih.gov/ and/or accessed upon direct request to M.E. Thomason (data) or L. Ji (code).

Acknowledgements

Moriah E. Thomason is primarily supported by grants from Foundation for the National Institutes of Health (Award ID: MH110793, DA050287, MH122447, ES032294).

Appendix A. Supporting information

Supplementary data associated with this article can be found in the online version at doi:10.1016/j.dcn.2023.101326.

References

Adisetiyo, V., Jensen, J.H., Tabesh, A., Deardorff, R.L., Fieremans, E., Di Martino, A., Gray, K.M., Castellanos, F.X., Helpern, J.A., 2014a. Multimodal MR imaging of brain iron in attention deficit hyperactivity disorder: a noninvasive biomarker that responds to psychostimulant treatment? Radiology 272, 524–532.

Adisetiyo, V., Jensen, J.H., Tabesh, A., Deardorff, R.L., Fieremans, E., Martino, A.D., Gray, K.M., Castellanos, F.X., Helpern, J.A., 2014b. Multimodal MR imaging of brain iron in attention deficit hyperactivity disorder: a noninvasive biomarker that responds to psychostimulant treatment? Radiology 272, 524–532.

Aiello, M., Salvatore, E., Cachia, A., Pappatà, S., Cavaliere, C., Prinster, A., Nicolai, E., Salvatore, M., Baron, J.-C., Quarantelli, M., 2015. Relationship between simultaneously acquired resting-state regional cerebral glucose metabolism and functional MRI: a PET/MR hybrid scanner study. Neuroimage 113, 111–121.

Behzadi, Y., Restom, K., Liau, J., Liu, T.T., 2007. A component based noise correction method (CompCor) for BOLD and perfusion based fMRI. Neuroimage 37, 90–101.

Biswal, B.B., Mennes, M., Zuo, X.-N., Gohel, S., Kelly, C., Smith, S.M., Beckmann, C.F., Adelstein, J.S., Buckner, R.L., Colcombe, S., Dogonowski, A.-M., Ernst, M., Fair, D., Hampson, M., Hoptman, M.J., Hyde, J.S., Kiviniemi, V.J., Kötter, R., Li, S.-J., Lin, C.-P., Lowe, M.J., Mackay, C., Madden, D.J., Madsen, K.H., Margulies, D.S., Mayberg, H.S., McMahon, K., Monk, C.S., Mostofsky, S.H., Nagel, B.J., Pekar, J.J., Peltier, S.J., Petersen, S.E., Riedl, V., Rombouts, S.A.R.B., Rypma, B., Schlaggar, B.L., Schmidt, S., Seidler, R.D., Siegle, G.J., Sorg, C., Teng, G.-J., Veijola, J., Villringer, A., Walter, M., Wang, L., Weng, X.-C., Whitfield-Gabrieli, S., Williamson, P., Windischberger, C., Zang, Y.-F., Zhang, H.-Y., Castellanos, F.X., Milham, M.P., 2010. Toward discovery science of human brain function. Proc. Natl. Acad. Sci. 107, 4734–4739.

Brammerloh, M., Morawski, M., Friedrich, I., Reinert, T., Lange, C., Pelicon, P., Vavpetič, P., Jankuhn, S., Jäger, C., Alkemade, A., Balesar, R., Pine, K., Gavriilidis, F., Trampel, R., Reimer, E., Arendt, T., Weiskopf, N., Kirilina, E., 2021. Measuring the iron content of dopaminergic neurons in substantia nigra with MRI relaxometry. Neuroimage 239, 118255.

Brody, B.A., Kinney, H.C., Kloman, A.S., Gilles, F.H., 1987. Sequence of central nervous system myelination in human infancy. I. An autopsy study of myelination. J. Neuropathol. Exp. Neurol. 46, 283–301.

Cabral, L., Calabro, F., Foran, W., Parr, A., Ojha, A., Rasmussen, J., Ceschin, R., Panigrahy, A., Luna, B., 2023a. Multivariate and Regional Age-Related Change in Basal Ganglia Iron in Neonates. bioRxiv, 2023.2007. 2005.547821.

Cabral, L., Calabro, F.J., Rasmussen, J., Foran, W., Moore, L.A., Graham, A., O'Connor, T. G., Wadhwa, P.D., Entringer, S., Fair, D., Buss, C., Panigrahy, A., Luna, B., 2023b. Gestational and postnatal age associations for striatal tissue iron deposition in early infancy. Dev. Cogn. Neurosci. 63, 101286.

Calhoun, V.D., Adali, T., Giuliani, N., Pekar, J., Kiehl, K., Pearlson, G., 2006. Method for multimodal analysis of independent source differences in schizophrenia: combining gray matter structural and auditory oddball functional data. Hum. Brain Mapp. 27, 47–62.

Cao, M., He, Y., Dai, Z., Liao, X., Jeon, T., Ouyang, M., Chalak, L., Bi, Y., Rollins, N., Dong, Q., 2017. Early development of functional network segregation revealed by connectomic analysis of the preterm human brain. Cereb. Cortex 27, 1949–1963.

Carpenter, K.L., Li, W., Wei, H., Wu, B., Xiao, X., Liu, C., Worley, G., Egger, H.L., 2016. Magnetic susceptibility of brain iron is associated with childhood spatial IQ. Neuroimage 132, 167–174.

Cecilia, A., Patricio, P., Donna, C., Rakibul, H., Sussanne, R., Betsy, L., Bharat, B., 2022. Cognitive control inhibition networks in adulthood are impaired by early iron deficiency in infancy. NeuroImage: Clin. 35, 103089.

Connor, J.R., Menzies, S.L., 1996. Relationship of iron to oligondendrocytes and myelination. Glia 17, 83–93.

Correa, N.M., Eichele, T., Adalı, T., Li, Y.-O., Calhoun, V.D., 2010. Multi-set canonical correlation analysis for the fusion of concurrent single trial ERP and functional MRI. Neuroimage 50, 1438–1445.

Cortese, S., Angriman, M., Lecendreux, M., Konofal, E., 2012a. Iron and attention deficit/hyperactivity disorder: what is the empirical evidence so far? A systematic review of the literature. Expert Rev. Neurother. 12, 1227–1240.

Cortese, S., Azoulay, R., Castellanos, F.X., Chalard, F., Lecendreux, M., Chechin, D., Delorme, R., Sebag, G., Sbarbati, A., Mouren, M.-C., 2012b. Brain iron levels in attention-deficit/hyperactivity disorder: a pilot MRI study. World J. Biol. Psychiatry 13, 223–231.

Darki, F., Nemmi, F., Möller, A., Sitnikov, R., Klingberg, T., 2016. Quantitative susceptibility mapping of striatum in children and adults, and its association with working memory performance. Neuroimage 136, 208–214.

Daugherty, A.M., Haacke, E.M., Raz, N., 2015. Striatal iron content predicts its shrinkage and changes in verbal working memory after two years in healthy adults. J. Neurosci. 35, 6731–6743.

Ding, C., Han, Y., Jiang, J., 2020. Exploring the relevance between brain glucose metabolism and functional connectivity in Chinese cognitive dysfunctions' subjects using integrated resting-state PET/MRI images. 2020 42nd Annual International Conference of the IEEE Engineering in Medicine & Biology Society (EMBC), pp. 1096–1099.

DuPre, E., Salo, T., Ahmed, Z., Bandettini, P.A., Bottenhorn, K.L., Caballero-Gaudes, C., Dowdle, L.T., Gonzalez-Castillo, J., Heunis, S., Kundu, P., 2021. TE-dependent analysis of multi-echo fMRI with* tedana. J. Open Source Softw. 6, 3669.

Erikson, K.M., Jones, B.C., Beard, J.L., 2000. Iron deficiency alters dopamine transporter functioning in rat striatum. J. Nutr. 130, 2831–2837.

Friston, K.J., 2003. Statistical parametric mapping. Neurosci. Database.: Pract. Guide 237–250.

Gao, W., Zhu, H., Giovanello, K.S., Smith, J.K., Shen, D., Gilmore, J.H., Lin, W., 2009. Evidence on the emergence of the brain's default network from 2-week-old to 2-year-old healthy pediatric subjects. Proc. Natl. Acad. Sci. 106, 6790–6795.

Gao, W., Lin, W., Grewen, K., Gilmore, J.H., 2017. Functional connectivity of the infant human brain: plastic and modifiable. Neuroscientist 23, 169–184.

Georgieff, M.K., 2011. Long-term brain and behavioral consequences of early iron deficiency. Nutr. Rev. 69, S43–S48.

Groves, A.R., Beckmann, C.F., Smith, S.M., Woolrich, M.W., 2011. Linked independent component analysis for multimodal data fusion. Neuroimage 54, 2198–2217.

Haacke, E.M., Cheng, N.Y., House, M.J., Liu, Q., Neelavalli, J., Ogg, R.J., Khan, A., Ayaz, M., Kirsch, W., Obenaus, A., 2005. Imaging iron stores in the brain using magnetic resonance imaging. Magn. Reson. Imaging 23, 1–25.

Hametner, S., Endmayr, V., Deistung, A., Palmrich, P., Prihoda, M., Haimburger, E., Menard, C., Feng, X., Haider, T., Leisser, M., 2018. The influence of brain iron and myelin on magnetic susceptibility and effective transverse relaxation-A biochemical and histological validation study. Neuroimage 179, 117–133.

Hect, J.L., Daugherty, A.M., Hermez, K.M., Thomason, M.E., 2018. Developmental variation in regional brain iron and its relation to cognitive functions in childhood. Dev. Cogn. Neurosci. 34, 18–26.

Hernando, D., Vigen, K.K., Shimakawa, A., Reeder, S.B., 2012. R mapping in the presence of macroscopic B0 field variations. Magn. Reson. Med. 68, 830–840.

Jenkinson, M., Bannister, P., Brady, M., Smith, S., 2002. Improved optimization for the robust and accurate linear registration and motion correction of brain images. Neuroimage 17, 825–841.

Jenkinson, M., Beckmann, C.F., Behrens, T.E., Woolrich, M.W., Smith, S.M., 2012. Fsl. Neuroimage 62, 782–790.

Kalpouzos, G., Garzón, B., Sitnikov, R., Heiland, C., Salami, A., Persson, J., Bäckman, L., 2017. Higher striatal iron concentration is linked to frontostriatal underactivation and poorer memory in normal aging. Cereb. Cortex 27, 3427–3436.

Karavallil Achuthan, S., Coburn, K.L., Beckerson, M.E., Kana, R.K., 2023. Amplitude of low frequency fluctuations during resting state fMRI in autistic children. Autism Res. 16, 84–98.

Knickmeyer, R.C., Gouttard, S., Kang, C., Evans, D., Wilber, K., Smith, J.K., Hamer, R.M., Lin, W., Gerig, G., Gilmore, J.H., 2008. A structural MRI study of human brain development from birth to 2 years. J. Neurosci. 28, 12176–12182.

Kundu, P., Inati, S.J., Evans, J.W., Luh, W.-M., Bandettini, P.A., 2012. Differentiating BOLD and non-BOLD signals in fMRI time series using multi-echo EPI. Neuroimage 60, 1759–1770.

Kuzawa, C.W., Chugani, H.T., Grossman, L.I., Lipovich, L., Muzik, O., Hof, P.R., Wildman, D.E., Sherwood, C.C., Leonard, W.R., Lange, N., 2014. Metabolic costs and evolutionary implications of human brain development. Proc. Natl. Acad. Sci. 111, 13010–13015.

Langkammer, C., Krebs, N., Goessler, W., Scheurer, E., Ebner, F., Yen, K., Fazekas, F., Ropele, S., 2010. Quantitative MR imaging of brain iron: a postmortem validation study. Radiology 257, 455–462.

Langkammer, C., Krebs, N., Goessler, W., Scheurer, E., Yen, K., Fazekas, F., Ropele, S., 2012. Susceptibility induced gray–white matter MRI contrast in the human brain. Neuroimage 59, 1413–1419.

Larsen, B., Luna, B., 2015. In vivo evidence of neurophysiological maturation of the human adolescent striatum. Dev. Cogn. Neurosci. 12, 74–85.

Larsen, B., Bourque, J., Moore, T.M., Adebimpe, A., Calkins, M.E., Elliott, M.A., Gur, R. C., Gur, R.E., Moberg, P.J., Roalf, D.R., 2020a. Longitudinal development of brain iron is linked to cognition in youth. J. Neurosci. 40, 1810–1818.
Larsen, B., Olafsson, V., Calabro, F., Laymon, C., Tervo-Clemmens, B., Campbell, E., Minhas, D., Montez, D., Price, J., Luna, B., 2020b. Maturation of the human striatal dopamine system revealed by PET and quantitative MRI. Nat. Commun. 11, 846.
Li, J., Kong, R., Liégeois, R., Orban, C., Tan, Y., Sun, N., Holmes, A.J., Sabuncu, M.R., Ge, T., Yeo, B.T.T., 2019. Global signal regression strengthens association between resting-state functional connectivity and behavior. Neuroimage 196, 126–141.
Lozoff, B., 2011. Early iron deficiency has brain and behavior effects consistent with dopaminergic dysfunction. J. Nutr. 141, 740S–746S.
Lozoff, B., Beard, J., Connor, J., Felt, B., Georgieff, M., Schallert, T., 2006. Long-lasting neural and behavioral effects of iron deficiency in infancy. Nutr. Rev. 64, S34–S43.
Ning, N., Zhang, L., Gao, J., Zhang, Y., Ren, Z., Niu, G., Dai, Y., Wu, E.X., Guo, Y., Yang, J., 2014. Assessment of iron deposition and white matter maturation in infant brains by using enhanced T2 star weighted angiography (ESWAN): R2* versus phase values. PloS One 9, e89888.
Ning, N., Liu, C., Wu, P., Hu, Y., Zhang, W., Zhang, L., Li, M., Gho, S.-M., Kim, D.-H., Guo, H., Yang, J., Jin, C., 2019. Spatiotemporal variations of magnetic susceptibility in the deep gray matter nuclei from 1 month to 6 years: A quantitative susceptibility mapping study. J. Magn. Reson. Imaging 49, 1600–1609.
Ortega, R., Cloetens, P., Devès, G., Carmona, A., Bohic, S., 2007. Iron storage within dopamine neurovesicles revealed by chemical nano-imaging. PloS One 2, e925.
Petanjek, Z., Judaš, M., Šimić, G., Rašin, M.R., Uylings, H.B., Rakic, P., Kostović, I., 2011. Extraordinary neoteny of synaptic spines in the human prefrontal cortex. Proc. Natl. Acad. Sci. 108, 13281–13286.
Power, J.D., Barnes, K.A., Snyder, A.Z., Schlaggar, B.L., Petersen, S.E., 2012. Spurious but systematic correlations in functional connectivity MRI networks arise from subject motion. Neuroimage 59, 2142–2154.
Raab, P., Ropele, S., Bültmann, E., Salcher, R., Lanfermann, H., Wattjes, M.P., 2022. Analysis of deep grey nuclei susceptibility in early childhood: a quantitative susceptibility mapping and R2* study at 3 Tesla. Neuroradiology 1–11.
Reinert, A., Morawski, M., Seeger, J., Arendt, T., Reinert, T., 2019. Iron concentrations in neurons and glial cells with estimates on ferritin concentrations. BMC Neurosci. 20 (1), 14.
Rouault, T.A., 2013. Iron metabolism in the CNS: implications for neurodegenerative diseases. Nat. Rev. Neurosci. 14, 551–564.
Sala-Llonch, R., Pena-Gomez, C., Arenaza-Urquijo, E.M., Vidal-Piñeiro, D., Bargallo, N., Junque, C., Bartres-Faz, D., 2012. Brain connectivity during resting state and subsequent working memory task predicts behavioural performance. Cortex 48, 1187–1196.
Salami, A., Avelar-Pereira, B., Garzón, B., Sitnikov, R., Kalpouzos, G., 2018. Functional coherence of striatal resting-state networks is modulated by striatal iron content. Neuroimage 183, 495–503.
Schenck, J.F., Zimmerman, E.A., 2004. High-field magnetic resonance imaging of brain iron: birth of a biomarker? NMR Biomed.: Int. J. Devoted Dev. Appl. Magn. Reson. In Vivo 433–445.
Shi, F., Salzwedel, A.P., Lin, W., Gilmore, J.H., Gao, W., 2017. Functional brain parcellations of the infant brain and the associated developmental trends. Cereb. Cortex 28, 1358–1368.
Smith, S.M., 2002. Fast robust automated brain extraction. Hum. Brain Mapp. 17, 143–155.
Stiernman, L.J., Grill, F., Hahn, A., Rischka, L., Lanzenberger, R., Panes Lundmark, V., Riklund, K., Axelsson, J., Rieckmann, A., 2021. Dissociations between glucose metabolism and blood oxygenation in the human default mode network revealed by simultaneous PET-fMRI. Proc. Natl. Acad. Sci. 118, e2021913118.
Sui, J., He, H., Yu, Q., Chen, J., Rogers, J., Pearlson, G.D., Mayer, A., Bustillo, J., Canive, J., Calhoun, V.D., 2013. Combination of resting state fMRI, DTI, and sMRI data to discriminate schizophrenia by N-way MCCA+ jICA. Front. Hum. Neurosci. 7, 235.
Tamura, T., Goldenberg, R.L., Hou, J., Johnston, K.E., Cliver, S.P., Ramey, S.L., Nelson, K.G., 2002. Cord serum ferritin concentrations and mental and psychomotor development of children at five years of age. J. Pediatr. 140, 165–170.
Tang, S., Xu, Y., Liu, X., Chen, Z., Zhou, Y., Nie, L., He, L., 2021. Quantitative susceptibility mapping shows lower brain iron content in children with autism. Eur. Radiol. 31, 2073–2083.
Tomasi, D., Volkow, N.D., 2018. Association between brain activation and functional connectivity. Cereb. Cortex 29, 1984–1996.
Wang, Y., Lu, Y., Du, M., Hussein, N.M., Li, L., Wang, Y., Mao, C., Chen, T., Chen, F., Liu, X., 2022. Altered spontaneous brain activity in left-behind children: a resting-state functional MRI study. Front. Neurol. 13, 834458.
Ward, R.J., Zucca, F.A., Duyn, J.H., Crichton, R.R., Zecca, L., 2014a. The role of iron in brain ageing and neurodegenerative disorders. Lancet Neurol. 13, 1045–1060.
Ward, R.J., Zucca, F.A., Duyn, J.H., Crichton, R.R., Zecca, L., 2014b. The role of iron in brain ageing and neurodegenerative disorders. Lancet Neurol. 13, 1045–1060.
Wedderburn, C.J., Ringshaw, J.E., Donald, K.A., Joshi, S.H., Subramoney, S., Fouche, J.-P., Stadler, J.A.M., Barnett, W., Rehman, A.M., Hoffman, N., Roos, A., Narr, K.L., Zar, H.J., Stein, D.J., 2022. Association of maternal and child anemia with brain structure in early life in South Africa. JAMA Netw. Open 5 e2244772-e2244772.
Whitfield-Gabrieli, S., Nieto-Castanon, A., 2012. Conn: a functional connectivity toolbox for correlated and anticorrelated brain networks. Brain Connect. 2, 125–141.
Yu-Feng, Z., Yong, H., Chao-Zhe, Z., Qing-Jiu, C., Man-Qiu, S., Meng, L., Li-Xia, T., Tian-Zi, J., Yu-Feng, W., 2007. Altered baseline brain activity in children with ADHD revealed by resting-state functional MRI. Brain Dev. 29, 83–91.
Zachariou, V., Bauer, C.E., Seago, E.R., Raslau, F.D., Powell, D.K., Gold, B.T., 2020. Cortical iron disrupts functional connectivity networks supporting working memory performance in older adults. Neuroimage 223, 117309.
Zang, Y.-F., Yong, H., Chao-Zhe, Z., Qing-Jiu, C., Man-Qiu, S., Meng, L., Li-Xia, T., Tian-Zi, J., Yu-Feng, W., 2007. Altered baseline brain activity in children with ADHD revealed by resting-state functional MRI. Brain Dev. 29, 83–91.
Zhang, Y., Shi, J., Wei, H., Han, V., Zhu, W.-Z., Liu, C., 2019. Neonate and infant brain development from birth to 2 years assessed using MRI-based quantitative susceptibility mapping. Neuroimage 185, 349–360.
Zou, Q.-H., Zhu, C.-Z., Yang, Y., Zuo, X.-N., Long, X.-Y., Cao, Q.-J., Wang, Y.-F., Zang, Y.-F., 2008. An improved approach to detection of amplitude of low-frequency fluctuation (ALFF) for resting-state fMRI: fractional ALFF. J. Neurosci. Methods 172, 137–141.
Zuo, X.-N., Di Martino, A., Kelly, C., Shehzad, Z.E., Gee, D.G., Klein, D.F., Castellanos, F. X., Biswal, B.B., Milham, M.P., 2010. The oscillating brain: complex and reliable. Neuroimage 49, 1432–1445.